Unraveling the effect of low Cu2O loading on P25 TiO2 and its self-reduction during methanol photoreforming

Fernando Plascencia-Hernández, Elim Albiter, Ghazzal Mohamed Nawfal, Christophe Colbeau-Justin, Hynd Remita, Heriberto Pfeiffer, Miguel A Valenzuela

Inorganic Chemistry Communications 158 (2023) 111541

Contents lists available at ScienceDirect

Inorganic Chemistry Communications

journal homepage: www.elsevier.com/locate/inoche

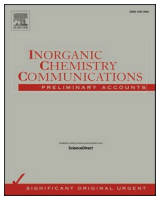

Short communication

Unraveling the effect of low Cu_2O loading on P25 TiO_2 and its self-reduction during methanol photoreforming

Fernando Plascencia-Hernández [a,b,d,*], Elim Albiter [b], Ghazzal Mohamed Nawfal [c], Christophe Colbeau-Justin [c], Hynd Remita [c], Heriberto Pfeiffer [d], Miguel A. Valenzuela [b,*]

[a] Centro de Investigación en Ciencia Aplicada y Tecnología Avanzada Unidad Legaria, Instituto Politécnico Nacional. Legaria 694, Col. Irrigación, 11500 CDMX, México
[b] Laboratorio de Catálisis y Materiales. ESIQIE- Instituto Politécnico Nacional. Zacatenco, 07738 México, CDMX, México
[c] Institut de Chimie Physique, UMR 8000 CNRS, Université Paris-Saclay, Orsay 91405, France
[d] Instituto de Investigaciones en Materiales, Universidad Nacional Autónoma de México. Circuito exterior s/n, Ciudad Universitaria, Del. Coyoacán, CP 04510 CDMX, México

ARTICLE INFO

Keywords:
Cu_2O/TiO_2 composites
Methanol photoreforming
Copper oxide reduction
Simulated solar light

ABSTRACT

Using noble metal-free catalysts is highly promising for sunlight-driven photocatalytic H_2 production. Copper compounds have gained considerable interest in this regard. Cu_2O/semiconductor composites exhibit superior photocatalytic activity compared to individual compounds. This study focuses on different Cu_XO/TiO_2 composites synthesized via chemical reduction, using Cu_2O weight ratios ranging from 1 to 0.05 concerning the TiO_2 source. Characterization techniques were employed, including XRD, SEM, XPS, UV–Vis DRS, PL, and TRMC. Surface modification of TiO_2 with Cu species (CuO, Cu_2O, and Cu^0) was observed during the photocatalytic reforming of methanol under simulated solar light. By loading small amounts of Cu_XO (0.05–0.1%) on TiO_2, the highest H_2 production and methanol mineralization were achieved, along with the formation of metallic copper. The coexistence of the Cu species and TiO_2 facilitated the effective separation of photogenerated electrons and holes, promoting the photoreduction of protons and photooxidation of methanol, respectively.

1. Introduction

The increasing population and energy demand on our planet have resulted in excessive consumption of fossil fuels, leading to higher greenhouse gas emissions and global warming. To address this issue, transitioning to carbon-free energy sources like hydrogen (H_2) is considered a viable alternative. Hydrogen possesses excellent properties, including high energy content, non-toxicity, and clean combustion, producing only water as a byproduct [1]. Solar energy conversion to hydrogen through photo-assisted processes appears to be a promising method [2].

There are two photocatalytic approaches for hydrogen generation: water splitting and reforming of organic compounds [3,4]. Water splitting involves using semiconductors to enable the reduction and oxidation of water molecules, generating hydrogen and oxygen. Photoreforming organic compounds like methanol, ethanol, or glycerol in the presence of semiconductors is an attractive option as it combines oxidation of the organic compound and reduction of protons to produce hydrogen. This approach prevents the unwanted reaction between hydrogen and oxygen [5].

Titanium dioxide (TiO_2) is the most extensively studied catalyst for photoreforming organic compounds. It offers advantages such as high oxidative power, chemical stability, affordability, and environmental friendliness. However, TiO_2 has limitations, including a high band gap that requires UV light for activation and fast recombination of electron-hole pairs. Therefore, researchers have explored various methods to enhance the photocatalytic activity of TiO_2 under visible light, such as surface modification, band gap modification, metal doping, and semiconductor coupling [6,7].

One effective strategy is to create a heterojunction by combining TiO_2 with other semiconductors like copper oxides (CuO, Cu_2O). This heterojunction facilitates the separation of photoinduced electrons and holes, improving photocatalytic performance. Cu_2O, with its suitable band gap and wide absorption coefficient in the visible spectrum, has been extensively studied for its potential applications in solar cells, gas sensors, and water splitting. Furthermore, due to their staggered gap,

* Corresponding authors at: Centro de Investigación en Ciencia Aplicada y Tecnología Avanzada Unidad Legaria, Instituto Politécnico Nacional. Legaria 694, Col. Irrigación, 11500 CDMX, México (Fernando Plascencia-Hernández).
E-mail addresses: fernandoplascenciah@gmail.com (F. Plascencia-Hernández), mavalenz@ipn.mx (M.A. Valenzuela).

https://doi.org/10.1016/j.inoche.2023.111541
Received 1 August 2023; Received in revised form 29 September 2023; Accepted 1 October 2023
Available online 2 October 2023

Cu_2O/TiO_2 heterojunctions have shown promising results in various reactions, enabling charge separation between the two semiconductors [8–10]. Muscetta et al. [11] coupled Cu_2O and TiO_2 (P25) systems from commercial sources using a ball-milling process and analyzing the Cu_2O load. This composite was tested for hydrogen production using methanol as a sacrificial agent, where it was concluded that 1 wt% of Cu_2O is the optimal load to reach the high H_2 production. On the other hand, a comparable approach was explored in glycerol photoreforming, as outlined in [12]. Here, different Cu_2O loads and CuO (3%) on TiO_2 were combined through the ball-milling method, demonstrating the heterojunction formation by photoelectrochemical characterizations and being 3% of Cu_2O the optimal copper oxide load toward H_2 production. Other parameters have been explored, such as the exposed facets-defects engineering [13] and Cu_2O morphology control [14] for the same Cu_2O/TiO_2 system.

In this study, Cu_2O-CuO particles were combined with P25 TiO_2 in different weight ratios to explore their synergistic effect on the photocatalytic performance of methanol photoreforming. Surprisingly, the irradiation with a solar simulator resulted in simultaneous methanol photo-reforming and self-reduction of copper oxides to metallic copper (Cu^0). Furthermore, this self-reduction process created a highly reductive environment, positively affecting hydrogen generation. The reasons behind this self-reduction process were attributed to several combined factors involving the Cu_XO-TiO_2 system and reaction conditions.

2. Materials and methods

2.1. Materials

Copper (II) chloride ($CuCl_2$; 97%), sodium hydroxide (NaOH; 98.2%), L-ascorbic acid (99.5%), polivinilpilorridone (PVP; M_W 40,000), titanium dioxide P25 Degussa (P25 TiO_2; 99.5%) were purchased from Aldrich and used without further purification. Aqueous solutions were prepared using deionized water (Milli-Q with 18.6 MΩ), ethanol reagent grade (denatured), and methanol reagent grade.

2.2. Synthesis of Cu_XO (X = 1, 2) polyhedral microparticles

Cu_XO polyhedral particles were synthesized at room temperature under a chemical reduction route with slight modifications [15]. First, sodium hydroxide solution (1 M, 40 mL) was prepared and stirred vigorously. Copper chloride solution (0.15 M, 40 mL) was added dropwise to the sodium hydroxide solution and stirred for 15 min. After that, 60 mL of PVP and L-ascorbic acid solution (1.42 wt ratio) was suddenly added to the last solution and stirred for 30 min. The obtained Cu_XO polyhedral particles were washed three times with a 1:1 water: ethanol solution and dried under air for storage.

2.3. Synthesis of Cu_XO/TiO_2 composites

Cu_XO polyhedral particles and P25 TiO_2 nanoparticles were dispersed separately in two ethanol: water 0.6:1 v:v solutions. Next, P25 TiO_2 solution was added dropwise to the Cu_XO solution under vigorous stirring until to obtain a homogeneous solution. Then, it was dried in the air, and the final powder was stored. Under this procedure, four composites were synthesized with the nominal Cu_XO/TiO_2 weight ratio indicated and labeled as follows: 0.05-Cu/Ti, 0.1-Cu/Ti, 0.5-Cu/Ti, and 1-Cu/Ti.

2.4. Characterization techniques

The characterization of the composites and single oxides was accomplished through several techniques. First, X-ray diffraction (XRD) was recorded from 15 to 80°, with a scan rate of 2° min^{-1}, using a Rigaku ULTIMA IV diffractometer in Bragg–Brentano geometry (Cu-$K_{\alpha 1}$ radiation, $\lambda = 1.540562$ Å) and nickel filter. Then, the morphology and particle size were determined by scanning electron microscopy (SEM), carried out on a JEOL 7800F microscope without any previous treatment. Furthermore, the samples were analyzed by energy dispersive spectroscopy (EDS) to identify the relative abundance of Cu, Ti, and O. These measurements were performed on four sample areas, calculating the average %wt of each element. Next, X-ray photoelectron spectroscopy (XPS) measurements were performed using a K–Alpha from Thermo Fisher Scientific X-ray photoelectron spectrometer with a monochromatic Al Kα X-ray source (1486.6 eV) and a base pressure of $1x10^{-9}$ Torr in the analytical chamber. The binding energy values were calibrated by contaminant carbon using the C 1s position at 285 eV. UV–vis diffuse reflectance spectroscopy (DRS) was measured on a GBC Cintra 20 spectrometer in the 200–800 nm range.

The samples were also analyzed by photoluminescence (PL) spectroscopy by using an FLS1000 spectrophotometer (Edinburg Instruments). The employed excitation wavelength was 325 nm, and the emission of the samples was captured from 420 to 800 nm at room temperature. Each spectrum was acquired using a spectral resolution of 0.5 nm and five accumulations of 0.1 s at each point. Finally, charge-carrier dynamic experiments were carried out through Time Resolved Microwave Conductivity (TRMC) using an incident microwave generated by a Gunn diode of the Kα band at 30 GHz. As a pulse light source, a laser (EKSPLA, NT342B) tunable between 220 and 2000 nm, equipped with an optical parametric oscillator (OPO) was used, delivering 8-ns FWMH pulses with a frequency of 10 Hz. Three excitation wavelengths were selected: 360, 470, and 520 nm, with a light energy density of 2.6 mJ cm^{-2}.

2.5. Photocatalytic evaluation

The photocatalytic evaluation proceeded as follows. The P25 TiO_2 Degussa, Cu_XO particles, and Cu_XO/TiO_2 composites were tested in a batch reaction system using a methanol–water mixture (MeOH: H_2O, 1:10; v:v) as the reaction medium. The photocatalyst concentration was fixed at 1 g L^{-1} in the reaction volume. Previously, the oxygen inside the reactor was eliminated by purging with N_2 gas for 15 min. Subsequently, the mixture was stirred in the dark for 30 min to establish an adsorption–desorption equilibrium between the catalyst and the methanol–-water solution. The reactor was then exposed to light from a Hg-Xe lamp with a power of 150 W for 8 h at room temperature. The H_2 production was monitored hourly using a gas chromatograph (Perkin Elmer Clarus 480) equipped with a TCD detector. Each evaluation was repeated three times. Following a similar procedure, the water-splitting reaction and the impact of photocatalyst concentration were investigated using the composite with the highest photoactivity. Additionally, cyclic experiments were conducted to assess the stability of this composite. In these cycles, the photocatalyst was recovered through centrifugation after the initial evaluation, redissolved in a fresh methanol–water solution (MeOH: H_2O, 1:10), and continued with subsequent cycles.

3. Results

3.1. XRD characterization

The diffraction patterns of the synthesized materials are displayed in Fig. 1. The diffraction peaks in the copper particles at 29.6, 36.5, 42.4, 52.6, 61.6, 73.7, and 77.5° of 2θ correspond to the cuprite structure of Cu_2O phase, according to JCPDS No. 01–073-6371, as expected. Furthermore, small peaks located at 35.7 and 38.3° were also detected, which can be attributed to the CuO phase (JCPDS No. 00–005-0667). Hence, the copper particles are composed of both Cu_2O and CuO, the last in less proportion concerning the Cu_2O. For the Cu_2O particles, the crystallite size (D) was determined using the XRD peak located at 36.5° through the Scherrer equation (Eq. (1), where $\lambda = 1.5406\ x10^{-10}$ m, B is the peak width, and θ represents the Bragg angle of the peak used. Thus, the crystallite size of the Cu_2O particles was calculated as 19 nm.

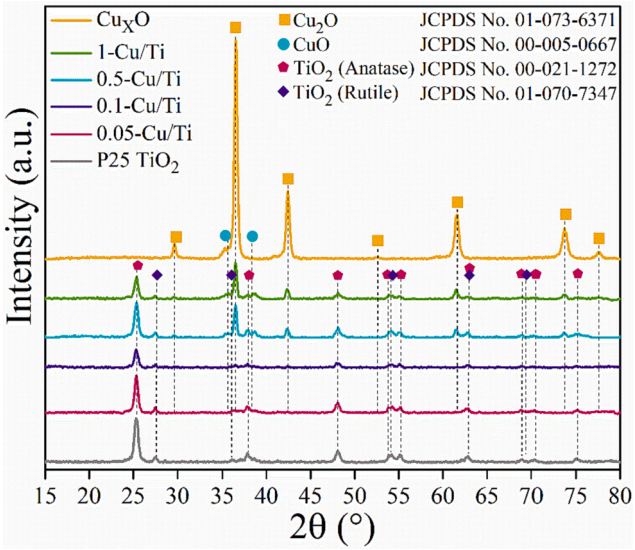

Fig. 1. X-ray diffraction patterns of Cu_XO particles, Cu_XO/TiO_2 composites, and commercial P25 TiO_2.

$$D = \frac{0.9*\lambda}{B*\cos\theta} \quad (1)$$

As Cu_2O and CuO are presented in the copper particles, they were labeled as Cu_XO. In the Cu_XO/TiO_2 composites, moreover, the peaks attributed to the Cu_XO particles showed the typical patterns corresponding to the anatase (A) and rutile (R) phases from P25 TiO_2, according to the JCPDS No. 00–021-1272 and No. 01–070-7347 cards, respectively, which it was confirmed with the XRD pattern of commercial P25 TiO_2. The significant decrease in the highest Cu_2O diffraction peak intensity (36.5°) is worth noting, in agreement with the reduction of the composites' Cu/Ti weight ratio.

3.2. SEM characterization

After the structural characterization, microstructural properties were determined via SEM, as shown in Fig. 2. According to the first image (Fig. 2A), the Cu_XO particles present a polyhedral morphology, as was expected, with some agglomeration regions. The average size of these particles was calculated, measuring 100 particles, and determined as 196 nm. For the Cu/Ti composites, P25 TiO_2 nanoparticles randomly surround the Cu_XO particles. The micrograph of the 1-Cu/Ti composite (Fig. 2B), containing the highest Cu_XO content, enables the

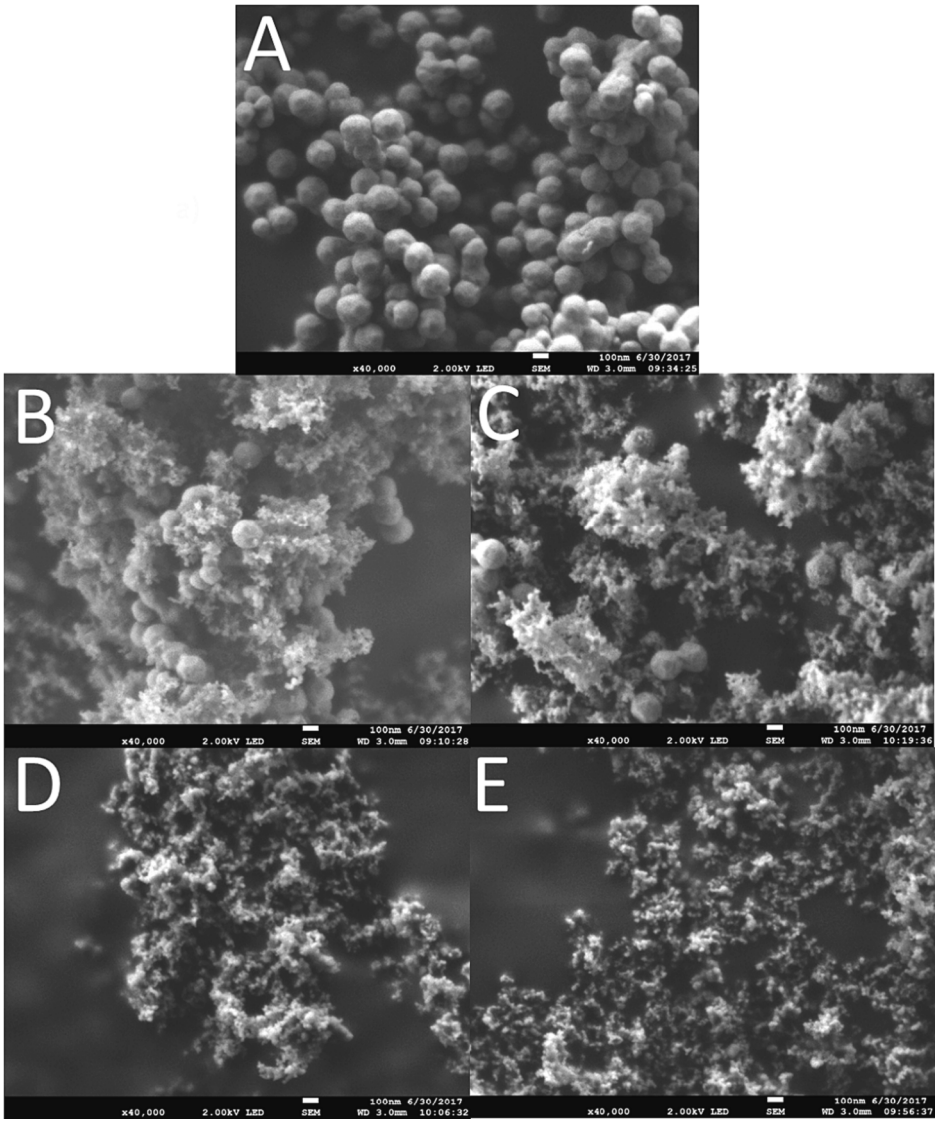

Fig. 2. SEM images of Cu_XO particles A) and the 1-Cu/Ti B), 0.5-Cu/Ti C), 0.1-Cu/Ti D), and 0.05-Cu/Ti E) composites.

identification of Cu_XO particles and P25 TiO_2, whose primary particle size has been reported as 21 nm. Fig. 2C shows the 0.5-Cu/Ti particles, where the Cu_XO particles remain visible, although their concentration is lower compared to the previous case. On the contrary, 0.1-Cu/Ti and 0.05-Cu/Ti composites shown in Fig. 2D and 2E, respectively, Cu_XO polyhedral particles were not identified due to their low proportion to the P25 TiO_2. However, the same configuration is expected, as was noted in the 0.1-Cu/Ti and 0.05-Cu/Ti composites, where P25 TiO_2 nanoparticles surround Cu_XO particles.

In addition, the composites' relative abundance of Cu, O, and Ti was determined through EDS measurements and compared to the expected weight percentage (Table 1). It is important to note that EDS is a semiquantitative technique, meaning the data obtained represents approximate values. The expected weight percentages were calculated based on the theoretical mass of each element in their respective initial oxides during the mixing process: Cu from Cu_2O (since CuO could not be precisely determined) and Ti from TiO_2. The calculated amounts of Cu and Ti were divided by the total quantity used by each oxide in the mixture. The expected oxygen amount was derived by subtracting the sum of the other elements (Cu and Ti) from 100%. While there were noticeable discrepancies between the desired and experimental results in some cases, a general trend emerged.

For copper, the experimental measurements generally followed the expected trend, with higher experimental values when the composite had a higher nominal Cu content. Regarding oxygen, the experimental results consistently showed higher values than the expected amounts across all composites, possibly due to the presence of CuO, which was detected by XRD (Fig. 1). However, like copper, the trend in experimental data aligned with the expected nominal values. In contrast, titanium exhibited lower observed weight percentages than the calculated nominal values. This discrepancy might be attributed to the loss of TiO_2 P25 particles during composite preparation, likely due to their small size and affinity for the glass material used in the mixing process. Nevertheless, the experimental trend followed the expected pattern, with lower experimental results corresponding to lower nominal Ti amounts and vice versa.

3.3. XPS characterization

The surface chemical composition and the chemical state of Cu within the 0.1-Cu/TiO_2 and 0.05-Cu/ TiO_2 composites were analyzed through XPS measurements. The survey spectra, as depicted in Fig. 3A, show four predominant elements: C, Ti, O, and Cu. The observed carbon signal is likely attributable to hydrocarbon contamination inherent to the XPS instrument or to adsorbed hydrocarbons from the ambient atmosphere, thereby serving as a reference signal. Peaks discerned at binding energies of 458.2 eV and 464.0 eV were assigned to the Ti $2p_{3/2}$ and Ti $2p_{1/2}$ transitions, respectively, as illustrated in Fig. 3B. The separation of 5.8 eV between these peaks is indicative of the stoichiometric nature of TiO_2 [16]. Fig. 3C presents the signals corresponding to the O 1s high-resolution spectrum. A deconvolution of this region showed two distinct peaks at 529.6 eV and 530.9 eV in both composites. The first signal is attributable to the oxygen integrated within the crystalline lattice of TiO_2. At the same time, the latter at 530.9 eV is ascribed to the oxygen atoms on the material's surface, most likely due to hydroxyl groups on the TiO_2 surface [17]. It is worth noting that the spectra did not exhibit discernible signals corresponding to Cu_XO species, likely due to their low concentration within the samples.

Fig. 3D and 3E show the Cu 2p high-resolution spectra of the 0.1-Cu/TiO_2 and 0.05-Cu/TiO_2 composites, respectively. The deconvolution of these spectra revealed the coexistence of Cu_2O and CuO phases in both composites. The presence of CuO was corroborated by the signals at 934.2 eV and 953.7 eV, corresponding to the Cu^{2+} $2p_{3/2}$ and Cu^{2+} $2p_{1/2}$ transitions, respectively [18]. The curves observed at 941.1 eV and 943.7 eV also correspond to the satellite peaks associated with the Cu^{2+} $2p_{3/2}$ transition. The Cu_2O phase was corroborated by the peaks at 932.4 eV and 952.4 eV of the Cu^{+} $2p_{3/2}$ and $2p_{1/2}$ transitions, respectively [18].

3.4. UV–vis diffuse reflectance spectroscopy characterization

Fig. 4 illustrates the UV–vis absorption spectra of Cu_XO particles, commercial P25 TiO_2, and Cu_XO/TiO_2 composites. The Cu_XO particles exhibited an absorption edge in the visible range (477–650 nm), while P25 TiO_2 displayed a distinct UV absorption band (325–410 nm). The Cu_XO/TiO_2 composites showed two bands, one in the UV region and another in the visible region, indicating absorption of photons across both spectra. The first band appeared between 325 and 330 nm for all composites, with the endpoint from 366 to 396 nm, aligning with the copper oxide content. The composite with the highest copper content (1-Cu/Ti) had the lowest endpoint value. The second band was observed around 477 nm in all composites, with the endpoint varying depending on the copper oxide content, ranging from 641 nm in the 1-Cu/Ti composite to 606 nm in the 0.05-Cu/Ti composite.

Moreover, the intensity of this band decreased as the weight ratio of Cu_XO particles increased. Higher copper oxide content resulted in a more intense absorption band. Thus, the copper oxide content influenced the absorption edge of both UV and visible bands. The UV band red-shifted with increased copper oxide content, while the visible band blue-shifted with decreased copper species, with the intensity being copper content-dependent. The band gap energy (E_g) of Cu_XO particles and commercial P25 TiO_2 was determined using the Kubelka-Munk and Tauc methods. The Kubelka-Munk function, Eq. (2), $F(R)$, relates to the absorption coefficient α and scattering coefficient S based on experimental diffuse reflectance (R) [19,20]. As S is nearly constant at any wavelength, $F(R)$ can be proportional to α [21]. The Tauc model established a relationship between the absorption coefficient and E_g, Eq. (3) [22], where h is the Planck's constant, ν is the frequency of the wavelength of the photon, A is a constant, and n is related to the band gap transition in the material. By combining these models, the experimental reflectance function could be associated with E_g Eq. (4). Plotting $(F(R)*h\nu)^{1/n}$ against the incident photon energy ($h\nu$) yielded the Tauc graph.

Because Cu_2O is the primary copper oxide phase in Cu_XO, a direct allowed transition (n = 1/2) was selected to calculate E_g [19]. Both direct allowed and forbidden transitions were compared, and the E_g value was determined as 2.34 eV, which closely matched the bulk Cu_2O value (2.17 eV) [23,24]. The blue shift in E_g can be attributed to the polyhedral morphology of Cu_XO particles, where the crystal facet structure influences their physical and optical properties. This behavior aligns with previous observations of similar Cu_2O particles [19,25,26]. For commercial P25 TiO_2, an indirect allowed transition (n = 2) was

Table 1
Relative abundance (%wt) of the elements in the composites determined by EDS and compared against nominal %wt.

Composite	Cu		O		Ti	
	Nominal (%wt)	Experimental (%wt)	Nominal (%wt)	Experimental (%wt)	Nominal (%wt)	Experimental (%wt)
1-Cu/Ti	45.67	44.17	25.24	28.86	29.09	26.97
0.5-Cu/Ti	30.49	26.39	30.16	32.77	39.34	40.85
0.1-Cu/Ti	8.51	8.91	37.30	41.18	54.19	49.91
0.05-Cu/Ti	4.46	5.45	38.62	45.33	56.92	49.22

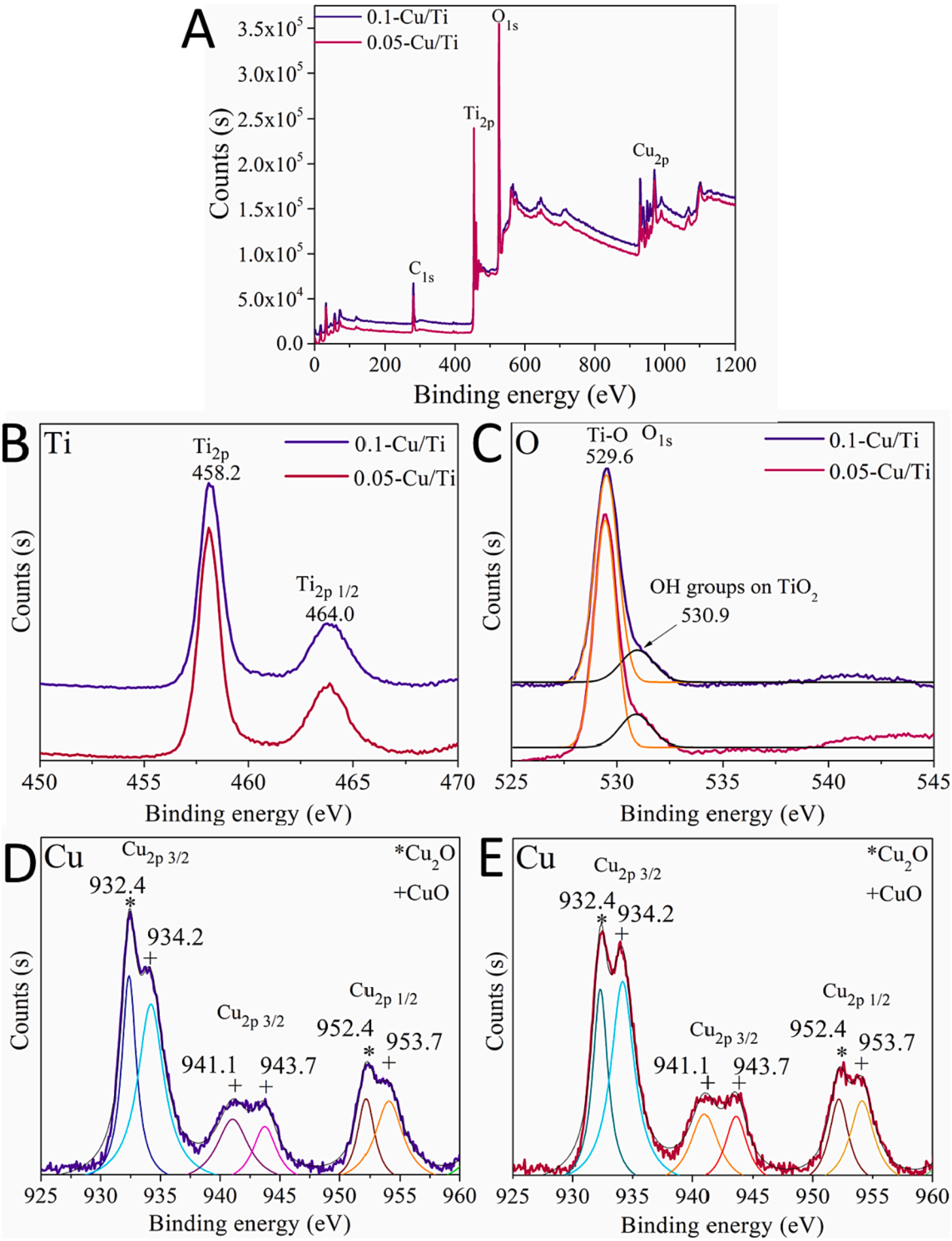

Fig. 3. XPS spectra of the 0.1-Cu/Ti and 0.05-Cu/Ti composites A), titanium region B), oxygen region C), copper region of the 0.1-Cu/Ti composite D), and copper region of the 0.05-Cu/Ti composite E).

chosen to calculate E_g, and the Y-axis was assigned as $(F(R)*h\nu)^{1/2}$. At F (R) = 0, the calculated E_g was 3.31 eV, consistent with previous literature [26]. Notably, the E_g of Cu/Ti composites (3.1–3.2 eV) was slightly lower than that of P25 TiO_2, as shown in Fig. 4

$$F(R) = \frac{(1-R)^2}{2*R} = \frac{\alpha}{S} \quad (2)$$

$$(\alpha*h\nu)^{\frac{1}{n}} = A(h\nu - E_g) \quad (3)$$

$$(F(R)*h\nu)^{\frac{1}{n}} = A(h\nu - E_g) \quad (4)$$

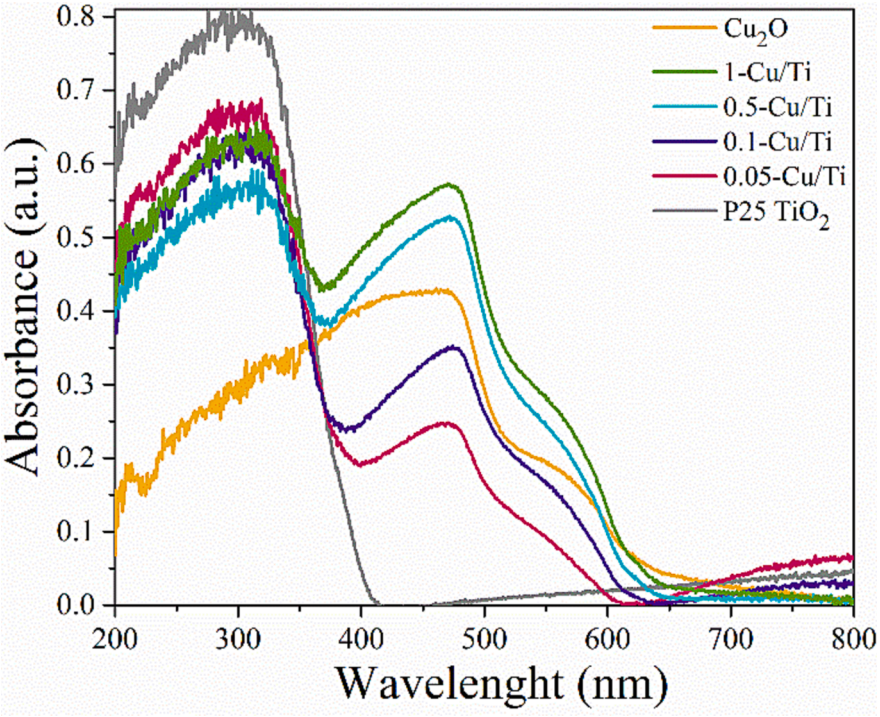

Fig. 4. Optical absorption spectra of Cu_XO particles, commercial P25 TiO_2, and Cu_XO/TiO_2 composites.

3.5. Photoluminescence and Time-Resolved microwave Conductivity analyses

The steady-state photoluminescence study was conducted to analyze the effect of copper oxide particles' addition to TiO_2 on charge (electron-hole) separation efficiency and the degree of their recombination. In the supporting information (Figure S1, Supporting Information), photoluminescence spectra of Cu_XO particles show three emission peaks between 500 and 700 nm, with the most intense at around 620 nm. Besides, as shown in Fig. 5, the P25 TiO_2 spectrum exhibits nine peaks in the 420–600 nm range that can be related to band edge-free excitons [27]. Note that when the copper oxide is added, a drastic decrease in the light emission signals of the spectrum is observed, although a similar profile is kept in all the cases. Furthermore, the peaks' intensity is according to the copper oxide amount on each composite. In the high-copper oxide content samples (0.5-1 wt%), significant signal decay is observed; meanwhile, when a small copper oxide load is added, the intensity did not decrease as in the high-content samples, and the profiles are similar between them (0.05 and 0.1 wt% Cu samples). These findings suggest that the degree of charge recombination reduction is directly contingent on the number of copper species on the TiO_2 surface.

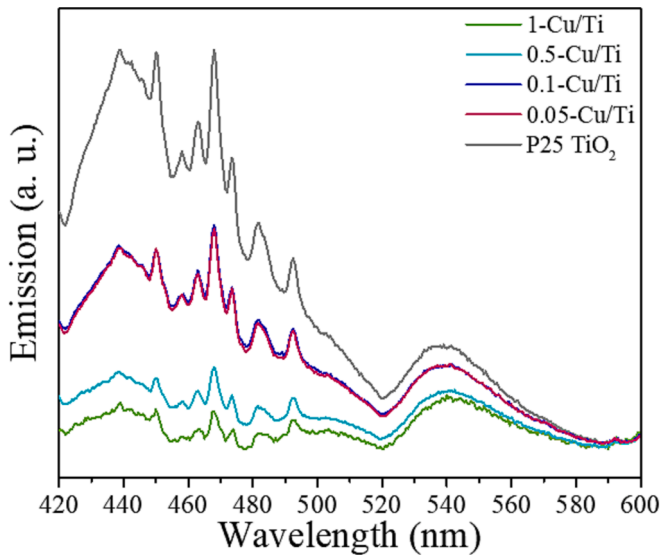

Fig. 5. Photoluminescence (PL) spectra P25 TiO_2 and Cu_XO/TiO_2 composites.

The TRMC signals were analyzed for Cu_XO, P25 TiO_2, and the coupled Cu_XO/TiO_2 (Figure S2). These signals correspond to the production of charge carriers immediately after laser excitation, followed by decay due to surface trapping, recombination, and surface reactions [28]. Cu_XO particles showed an intense TRMC signal in both UV and visible ranges, particularly in the visible spectrum. P25 TiO_2 produced photogenerated electrons under UV irradiation, but the TRMC signal was weaker in the visible range due to its higher band gap. The Cu_XO/TiO_2 composites exhibited an extended ability to produce charge carriers in the UV–visible range, with the signal intensity under visible wavelengths related to the Cu_XO proportion. Higher Cu_XO weight ratios resulted in more intense signals but faster decay. Lower Cu_XO ratios showed decreased signal intensity but more stable decay stages. In the composites, the generation of photoelectrons varied with the tested wavelengths. The 0.1-Cu/Ti composite slightly reduced photoelectron generation with wavelength. The 0.05-Cu/Ti composite showed the best photoelectron generation at 470 nm, and the coupled effect between copper oxides and titanium dioxide enhanced photoelectron generation at this specific wavelength.

3.6. Photocatalytic activity

It is essential to mention that, after the initial 30 min of irradiation, a notorious color change from slightly yellow to deep purple was observed (Fig. 6A), which was kept throughout the subsequent irradiation time. Surprisingly, when the irradiation was stopped, the reaction solution returned to its original slight yellow color after around 10 h. This phenomenon was observed in all the experiments and will be analyzed later. The evolved H_2 and CO_2 gases were measured every hour and up to 8 h of irradiation time. As shown in Fig. 6B, the Cu_XO polyhedral particles

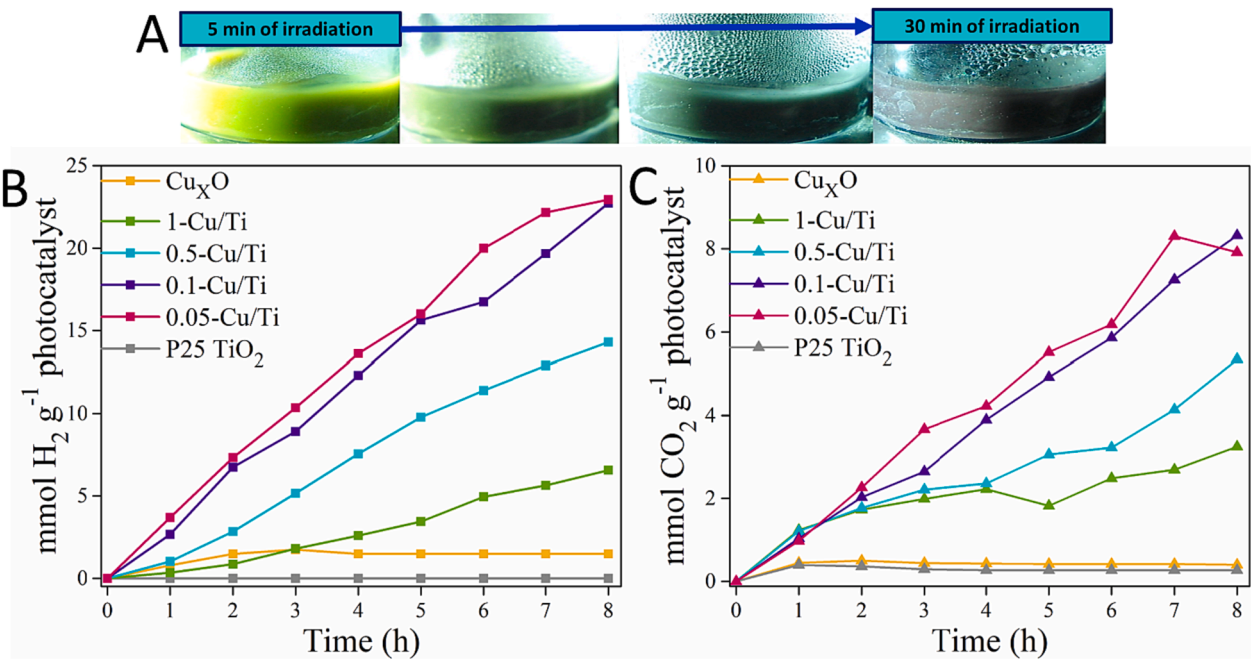

Fig. 6. Color change of the solution of reaction after 30 min of irradiation, and during the photocatalytic process A), H_2 production B) and CO_2 evolution C) by methanol photo-reforming under solar simulator at 150 W, with a concentration of 1 g L^{-1} of the photocatalyst.

did not present photocatalytic activity throughout the evaluation period due to the null H_2 production. For the commercial P25 TiO_2, low H_2 was produced after 8 h under UV–vis irradiation. Conversely, the Cu_XO/TiO_2 composites showed significant H_2 generation compared to every single oxide, the less-copper oxide composites, 0.1-Cu/Ti, and 0.05-Cu/Ti, the most active materials. Furthermore, their H_2 production rates increased almost eight times in these composites compared to the H_2 production rate of commercial P25 TiO_2.

On the other hand, the CO_2 generation was measured to verify the stoichiometry of the methanol-reforming reaction and corroborated that both H_2 and CO_2 could be consumed or produced in secondary reactions as water-splitting reactions in the H_2 production case. Fig. 6C revealed that the composite materials, concerning the single oxides, made higher CO_2 in the H_2 generation case. Furthermore, the CO_2 generated in the composites showed a similar tendency to the H_2 production, where the 0.1-Cu/Ti and 0.05-Cu/Ti composites produced the highest CO_2 amount. The CO_2 production rates with the 0.1-Cu/Ti and 0.05-Cu/Ti composites were fourteen times higher than the CO_2 production rate in commercial P25 TiO_2. According to the results presented in Table 2, the following set of reactions can occur to explain H_2 and CO_2 evolution:

$$CH_3OH \xrightarrow[k_1]{h\nu+pcat.} HCOH + H_2 \quad (5)$$

$$HCOH + H_2O \xrightarrow[k_2]{h\nu+pcat.} HCO_2H + H_2 \quad (6)$$

$$HCO_2H \xrightarrow[k_3]{h\nu+pcat.} CO_2 + H_2 \quad (7)$$

With the overall reaction being:

$$CH_3OH + H_2O \xrightarrow[K]{h\nu+pcat} CO_2 + 3H_2 \quad (8)$$

Where $h\nu$ is the photon energy, *pcat* is the photocatalyst, k_x is the rate constant of each reaction, and K is the global equilibrium constant. Therefore, in agreement with Eq. (8), the H_2/CO_2 molar ratio must be 3. However, the average molar ratio of the experimental data showed different values for both single oxides and the composites (Table 2). The H_2/CO_2 molar ratio calculated in the Cu_XO particles was 1.25, but as the evolution of both gases was almost negligible, the photocatalytic activity is considered null. In contrast, the composites showed H_2/CO_2 molar ratios between 2.39 and 2.9, indicating a variation of the H_2 production or CO_2 generation concerning the theoretical values expected by a secondary reaction. This result also relates to each material's copper oxide weight ratio, where the 0.05-Cu/Ti composite has a lower difference. This result can be explained by the process represented in the following equation;

$$CH_3OH + 2Cu_2O + CuO \xrightarrow{h\nu\ (\lambda=UV)} CO_2 + 2H_2O + 5Cu^0 \quad (9)$$

In this secondary process carried out under the irradiation time, methanol is oxidized to carbon dioxide and water; meanwhile, both copper oxides (Cu_2O and CuO) are reduced to metallic copper (Cu^0) [29,30]. After the irradiation is stopped, the oxidation environment and the presence of TiO_2 promote the re-oxidation of the metallic copper. This reaction can be an additional way for CO_2 generation, explaining the theoretically expected value of the H_2/CO_2 molar ratio lower than 3. Additionally, there is a direct dependence on the copper oxide content and the process, which should be why the H_2/CO_2 molar ratio was lesser in the composites with the higher Cu_XO content than in the composites with lower Cu_XO content. Thus, the process proposed in Eq. (9) favors

Table 2
H_2 and CO_2 evolution after 8 h irradiation time of methanol photoreforming.

Photocatalyst	H_2 mmol g^{-1}	H_2 evolution rate mmol $g^{-1}h^{-1}$	CO_2 mmol g^{-1}	CO_2 evolution rate mmol $g^{-1}h^{-1}$	Molar ratio H_2/CO_2
Cu_XO	0.05	0.007	0.04	0.01	1.25
1-Cu/Ti	6.21	0.69	2.59	0.29	2.39
0.5-Cu/Ti	14.29	1.79	5.34	0.67	2.67
0.1-Cu/Ti	22.72	2.84	8.32	1.04	2.73
0.05-Cu/Ti	22.94	2.86	7.91	0.99	2.90
P25 TiO_2	1.48	0.37	0.27	0.07	5.48

the composites with high copper oxide content, giving rise to a lower H_2/CO_2 molar ratio. This reaction also explains the change of color of the solution during the irradiation time. When the composites are irradiated, the process represented in Eq. (9) takes place, and the copper oxides in the composites are reduced to metallic copper, changing the color of the solution from the slightly yellow characteristic color of copper oxides to deep purple.

On the other hand, in commercial P25 TiO_2, the H_2/CO_2 molar ratio was almost double the theoretical value, around 5.48. In this case, the increment of the molar ratio is due to the increment of the H_2 production to the expected stoichiometric amount from the methanol photo-reforming. Therefore, the P25 TiO_2 can carry out a methanol photo-reforming reaction [31,32], and the additional H_2 amount can be produced by water splitting, which has been reported for this material previously [33].

For comparison purposes, the 0.1-Cu/Ti composite was evaluated in the water-splitting reaction, and the results are displayed in Fig. 7A. Notoriously, no H_2 evolution was detected in this reaction (water + composite + irradiation), which means that methanol photo-reforming is the reaction carried out for H_2 production. Methanol is a hole collector and can inject electrons in the conduction band (CB) of the Cu_XO/TiO_2 composite [34]. The release of the hydrogen radicals follows this dissociative adsorption of methanol. Thus, the hydrogen comes from the released protons after methanol photooxidation, following Eqs. (5)–(7). Furthermore, it is essential to mention that no color change was observed during the water-splitting evaluation, confirming the additional CO_2 generation process depicted in Eq. (9), where methanol is involved.

The photocatalyst concentration effect was studied with the same composite (0.1-Cu/Ti), using concentrations from 0.5 to 2 g L^{-1} (Fig. 7B). Methanol photo-reforming is highly sensitive at the catalyst concentration since the best photocatalytic performance was achieved using a 1 g L^{-1} catalyst concentration. Indeed, at low catalyst concentrations (i.e., 0.5 g L^{-1}), insufficient proton conversion sites are available to convert into molecular hydrogen. On the contrary, by increasing the catalyst load (1.5–2 g L^{-1}), a significant decrease in the H_2 production rate is observed, which is attributed to light scattering of the material hindering the illumination in the reaction system, as well as agglomeration-sedimentation of the photocatalyst, despite of the stirring of the solution of reaction [35,36].

Finally, in Fig. 7C, the cyclic capacity results of the 0.1-Cu/Ti composite are presented. The photoactivity of the material was kept after three reaction cycles; the maximum H_2 production on each cycle was between 15 and 17 mmol of H_2 per gram of photocatalyst. Despite an aqueous environment and irradiation for at least 24 h, this significative stability demonstrated that the Cu_XO/TiO_2 composites are good candidates to reuse more than once for methanol photo-reforming without losing their photocatalytic performance. Furthermore, it is essential to point out that the slight yellow color of the composite changed to deep purple on each reaction cycle. Then, after stopping the irradiation, washing and drying it, its color came back to a slight yellow as at the beginning of the reaction, before the irradiation. Thus, as a brief, the photoactivity was strongly susceptible to the Cu_XO amount in the composites, obtaining the best results at low Cu_XO concentrations (i.e.,

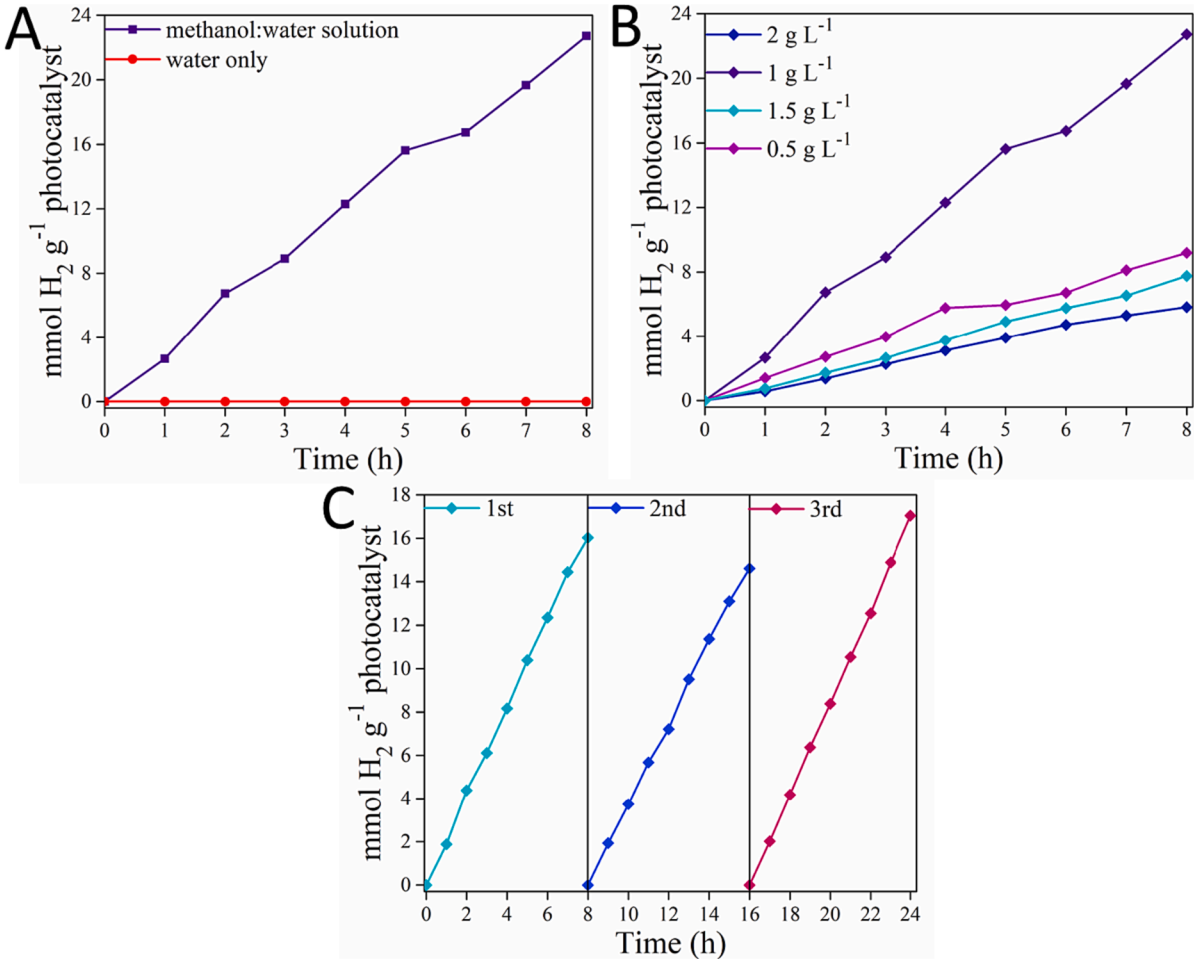

Fig. 7. Methanol photoreforming vs. water splitting processes A), the effect of the photocatalyst concentration B), and the reaction cycles C) in H_2 evolution for the 0.1-Cu/Ti composite.

0.1-Cu/Ti and 0.05-Cu/Ti composites). Then, an excess of the optimal amount of Cu_XO can promote the recombination of the photo charge carriers, decreasing the photoactivity [37]; moreover, the feasibility of the secondary oxidation process of methanol, where CO_2 and H_2O instead of H_2 are produced.

4. Discussion

The spatial distribution, composition, and electronic properties of Cu_XO/TiO_2 composites significantly impacted the methanol photoreforming process; hence, the description of its initial configuration is crucial to explain the composites' behavior. XRD data and SEM micrographs in Figs. 1 and 2 confirmed that Cu_XO and TiO_2 particles exist as separate phases but have random close contact without a specific configuration. This spatial distribution, represented in Fig. S3A, allows direct contact between Cu_XO and TiO_2 particles and the aqueous methanol solution. As a result, the photogenerated charge carriers from both semiconductors can participate in surface redox reactions during irradiation due to the high probability of charge transfer at the semiconductor-liquid interface [38].

Furthermore, it is essential to note the presence of four species (i.e., Cu_2O, CuO, TiO_2 anatase, and rutile) in the composites and their contribution to the electronic properties of the entire system. The first specie is Cu_2O, identified as polyhedral particles through XRD, SEM, and XPS techniques. Additionally, CuO was detected in the identical particles based on XRD patterns. XPS spectra of the 0.1-Cu/Ti and 0.05-Cu/Ti samples confirmed the presence of CuO as part of the composites. As reported elsewhere, CuO is likely formed as a thin layer over the surface oxidation of Cu_2O particles [39,40]. The third and fourth components are the anatase and rutile crystalline phases in commercial P25 TiO_2, with a standard proportion of 80:20 [38]. These phases were verified by XRD patterns in all composites.

Considering the species in the composites, the type of interactions between them is crucial. The most significant interaction arises from the coexistence of Cu_2O and TiO_2, forming a p-n heterojunction due to the nature of both semiconductors [41]. In the interface of the semiconductors, before irradiation, electrons from Cu_2O, a p-type semiconductor, migrate toward TiO_2, an n-type semiconductor, due to its small work function, reaching a Fermi level equilibrium. Thus, the Cu_2O remains positively charged and TiO_2 negatively charged, which induces an internal electric field [42], as reported by DFT results [43], shown in Fig. S3B.

Thus, based on the spatial distribution of particles and the presence of four species in the composites, a band alignment was proposed for the photocatalysts based on their band edge and E_g values (Fig. S3C). The Cu_2O band gap was calculated as 2.34 eV, slightly higher than the commonly reported values in the literature (around 2.2 eV) [44]. Despite this increase in E_g, the valence band (VB) and conduction band (CB) positions of Cu_2O, reported at 1.07 and −1.13 V [45], respectively, were considered in the proposed alignment. In the case of CuO, although its band gap was not experimentally determined, its E_g alignment was considered (VB and CB positions as 1.5 and −0.2 V relative to NHE, respectively) [46], as it is part of the Cu_2O particles and can contribute to the electronic properties of the composites. As for commercial P25 TiO_2, the E_g was estimated at 3.31 eV, composed of the E_g values of pure anatase (3.2 eV) and pure rutile (3.02 eV) [38]. The VB and CB positions of anatase were measured around 2.9 and −0.29 V relative to NHE [45], while the E_g position of rutile was identified close to anatase's CB and VB [42]. The proposed E_g positions for each component in the composite are represented based on these assumptions and taking into account the experimental determination reported previously [47].

Based on this initial state, a reaction pathway can be proposed upon irradiation of the composites with simulated solar light. The UV wavelength excites P25 TiO_2 particles, while visible light excites copper oxides (Cu_2O, CuO), generating electron-hole pairs in the semiconductors. The photogenerated charge carriers can migrate directly to the solid–liquid interphase due to the spatial distribution of particles and the Cu_XO-TiO_2 contact. In the latter case, as an internal electric field is formed in the p-n heterojunction, electrons migrate from Cu_XO to the TiO_2 CB, first to the anatase phase and then to the rutile phase, where an accumulation of charge carriers is possible [48]. Meanwhile, photogenerated holes can remain in the Cu_2O and CuO VB, and holes generated in the VB of P25 TiO_2 migrate to the Cu_2O VB according to the proposed band alignment, leading to spatial separation of charge carriers throughout the composite. This overall scheme of photo-redox reactions minimizes charge recombination, supported by semiconductor thermodynamics [42,49]. Additionally, the aqueous methanol plays an active role as a hole scavenger at this stage, preventing charge recombination and providing the protons and electrons required for H_2 production [32]. The evaluation section describes the general reaction Eq. (8), which can be rewritten as Eq. (10). According to this equation, the theoretical oxidation potential required is 0.02 V [50].

$$CH_3OH + H_2O \rightarrow CO_2 + 6H^+ + 6e^- \quad E^0 = 0.02\,V \tag{10}$$

In addition, as a secondary reaction, copper species were reduced due to methanol oxidation, resulting in a color change of the photocatalyst-aqueous methanol solution. Initially, the suspension is slightly yellow due to the Cu_XO-TiO_2 composites. However, after irradiation, the color gradually changes to ~~a~~ deep red–purple associated with metallic copper (Cu^0) [51,52]. Although clear evidence of Cu^0 presence was not found in the experimental analysis, the color change of the system, increased CO_2 evolution, and no color change during the water splitting test support this assumption. The difference in oxidation state is feasible based on the proposed band alignment. The reduction of Cu_2O to Cu^0 requires a potential of −0.360 V [53], which falls within the band gap of Cu_2O. Intense radiation can promote the self-reduction of Cu_2O to Cu^0 (Fig. S4A) by the photogenerated electrons [54].

Moreover, the high flux of charge carriers in the p-n heterojunction can increase the electron density in the P25 TiO_2 conduction band [49], which is close to the potential required for Cu^0 formation. The combined effect of the secondary methanol oxidation and the presence of electrons from Cu_2O or the p-n heterojunction can reduce copper species from Cu^{+2} and Cu^{+1} to Cu^0, as shown in Scheme 1A. The Cu^0/P25 TiO_2 system is proposed after irradiation, and the required reduction potential is represented in the optical band alignment of the initial species (Scheme 1B).

The presence of Cu^0 particles alters the charge transfer mechanism in the composites (Scheme 1C). A Schottky barrier is formed between Cu^0 and P25 TiO_2, leading to a decrease in the recombination rate of photocarriers. Electron transfer from P25 TiO_2 to Cu^0 particles is favored due to the metal's higher work function than the semiconductor. This electron migration continues until equilibrium is reached, aligning the Fermi levels of Cu^0 and P25 TiO_2 with the conduction band of P25 TiO_2. As a result, P25 TiO_2 and Cu^0 particles acquire excess positive and negative charges, respectively [38,55]. This efficient separation of charge carriers promotes H^+ reduction, enhancing H_2 production according to Eq. (10).

Additionally, to the previously described process, the Cu_2O/CuO hybrid structure in the composites represents a double way to generate electrons [49], and the homojunction between anatase–rutile improves the charge separation [38,49,56]. Several hours after turning off the irradiation, the composites returned to the initial slight yellow from the red–purple color, indicating the oxidation state change from Cu^0 to copper oxides again, as shown in Figure S4(B-E). The following reactions show the likely path of the Cu^0 oxidation to the Cu_2O particles during the photocatalytic test and after irradiation, where P25 TiO_2 participates [54]:

$$TiO_2 \xrightarrow{h\nu} TiO_2 + h^+ + e^- \tag{11}$$

$$2H^+ + 2e^- \rightarrow H_2 \tag{12}$$

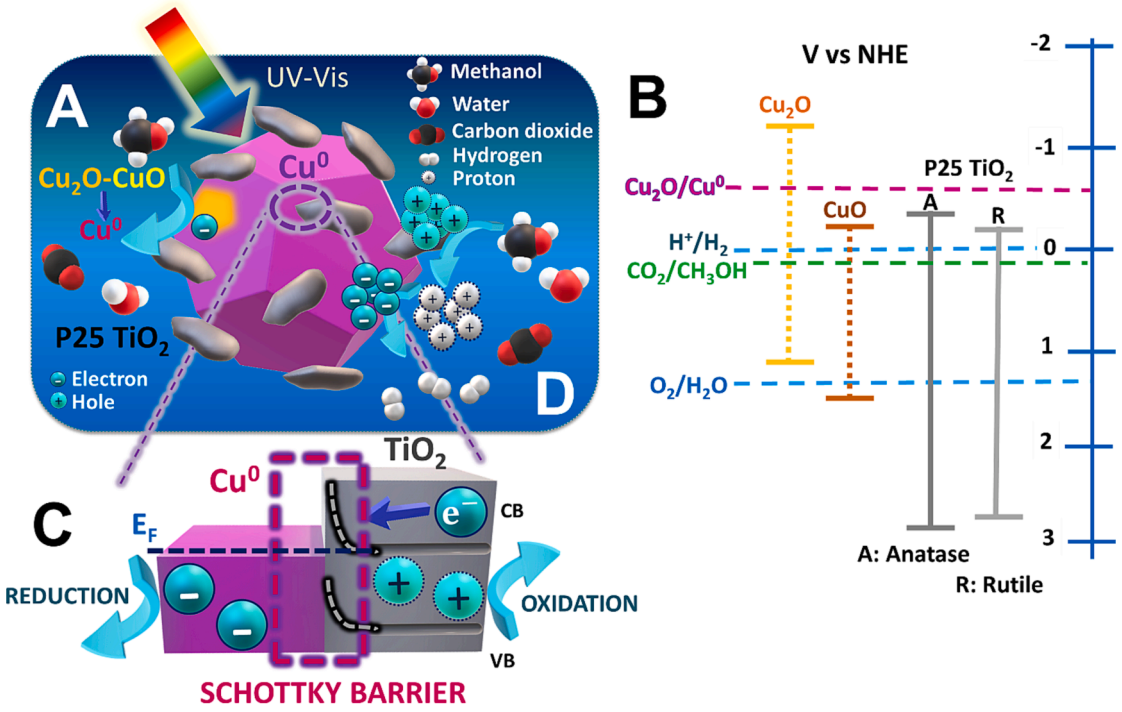

Scheme 1. The photocatalytic performance of the Cu_XO/TiO_2 composites during irradiation.

$$Cu^0 + h^+ \rightarrow Cu^{+1} + e^- \quad (13)$$

The remaining holes from P25 TiO_2 participate actively in the re-oxidation of Cu^0 to Cu_XO, playing a critical role in the copper re-oxidation process after irradiation [57,58]. To gain insight into the copper species present in the spent photocatalyst after 8 h of irradiation, we conducted XPS characterization of the 0.1-Cu/Ti composite (see Figure S5). When examining the high-resolution O 1s spectrum of the spent catalyst (Fig. S5A), we observed a subtle change in the signal associated with oxygen bound to the TiO_2 surface. This alteration is likely a result of the adsorption of additional oxygenated species, possibly stemming from the methanol used in the reaction. An analysis of the Cu 2p spectrum of the spent 0.1-Cu/Ti composite showed no significant change in the copper species present (Fig. S5B). However, there was a slight shift in their distribution, notably with a minor increase in the signal associated with Cu^{2+}.

Finally, a comparative table was performed between previous reports and the obtained results in the current work (Table S1). The system copper species-titanium dioxide has been widely studied due to the significative performance of the combination of these species during photocatalytic H_2 production through alcohol reforming. Among the strategies used, the modification of the copper oxide morphology, size, and ratio concerning titanium dioxide has been reported. Commercial P25 TiO_2 has been selected as a titanium source for the last one, although several groups have synthesized it, modifying its morphology and size. Also, different elements, such as silver, have been added to this kind of system. Besides, various sacrificial agents have been used for alcohol reforming, although, in most cases, methanol has shown the best results. Concerning the source light, the works reported a power between 100 and 500 W, with high-energy wavelengths in the UV region. Each case's maximum H_2 production rate is mainly linked to the alcohol proportion in the reaction medium and the structural properties of the oxides. The obtained values range from 0.009 to 286 mmol $g^{-1}h^{-1}$; however, most are between 2.048 and 4.5 mmol $g^{-1}h^{-1}$. This work's best H_2 production rate is in this range, being 2.86 mmol $g^{-1}h^{-1}$. This result could be considered exceptional, taking into account the easy synthesis method selected, low copper oxide ratio to P25 TiO_2 (0.05 to 1.0), methanol proportion used (1:10), and the lower power of the irradiation source (150 W), due to that similar or slightly higher results have been reported under complicated synthesis methods, higher alcohol proportion and high power of irradiation source.

5. Conclusions

Cu_XO/TiO_2 composites with different weight ratios were successfully synthesized using a simple, room-temperature wet-mixed method. These composites exhibited a specific spatial distribution, allowing both Cu_2O/CuO particles and the reaction solution to come into contact, facilitating their participation in redox reactions. In addition, the composites demonstrated photoactivity across a broad range of wavelengths, including the visible and UV regions, as confirmed by PL and TRMC measurements. In the methanol photo-reforming reaction, the synthesized composites also exhibited a Cu_2O/CuO species self-reduction to Cu^0, which was evident from the change in color of the photocatalyst-aqueous methanol solution. The self-reduction was attributed to the secondary oxidation reaction of methanol, leading to a decrease in the H_2/CO_2 molar ratio during the evaluation.

The formation of a p-n heterojunction facilitated the efficient spatial separation of electron-hole pairs, reducing copper oxides to metallic copper due to the high electron density and creating a Schottky barrier in the new Cu^0/P25 TiO_2 composite, generating a high density of negative charges and enhancing H_2 production by increasing proton availability in the reaction medium and improving stability. Furthermore, the photocatalytic content influenced the Cu_XO performance, with the number of active sites and phenomena like light scattering and sedimentation playing a critical role. In addition, the combination of spatial distribution, the presence of methanol, the p-n heterojunction, the Cu_XO/TiO_2 weight ratio, and the presence of four species, including the P25 TiO_2 homojunction, contributed to the self-improvement of the photocatalysts and enhanced photoactivity for H_2 production via methanol photoreforming.

Funding

This research was financed by Consejo Nacional de Ciencia y Tecnología México, project numbers 299909 and 807101, and also by Instituto Politécnico Nacional SIP projects 20230926 and 20230909.

CRediT authorship contribution statement

Fernando Plascencia-Hernández: Methodology, Writing – original draft, Investigation. **Elim Albiter:** Investigation, Resources, Writing – review & editing. **Ghazzal Mohamed Nawfal:** Investigation. **Christophe Colbeau-Justin:** Investigation. **Hynd Remita:** Investigation. **Heriberto Pfeiffer:** Investigation, Resources. **Miguel A. Valenzuela:** Supervision, Resources, Writing – review & editing.

Declaration of Competing Interest

The authors declare that they have no known competing financial interests or personal relationships that could have appeared to influence the work reported in this paper.

Data availability

Data will be made available on request.

Acknowledgments

This work is dedicated to the memory of our colleague Guadalupe Valverde Aguilar, who passed away in 2019 and provided valuable ideas. The authors thank Lourdes Bazán-Díaz (LUME, IIM-UNAM) for technical assistance. FPH is grateful for CONACyT and BEIFI (IPN) fellowships. MV and HR acknowledge Université Paris-Saclay for the financial support through the Chaire Jean d'Alembert program and the IRS MOMENTOM (Initiative de Recherche Stratégique).

Appendix A. Supplementary material

Supplementary data to this article can be found online at https://doi.org/10.1016/j.inoche.2023.111541.

References

[1] J.O. Abe, A.P.I. Popoola, E. Ajenifuja, O.M. Popoola, Hydrogen energy, economy and storage: Review and recommendation, Int. J. Hydrogen Energy 44 (2019) 15072–15086, https://doi.org/10.1016/j.ijhydene.2019.04.068.

[2] P. Nikolaidis, A. Poullikkas, A comparative overview of hydrogen production processes, Renew. Sustain. Energy Rev. 67 (2017) 597–611, https://doi.org/10.1016/j.rser.2016.09.044.

[3] M.E. El-Khouly, E. El-Mohsnawy, S. Fukuzumi, Solar energy conversion: From natural to artificial photosynthesis, J Photochem Photobiol C: Photochem Rev 31 (2017) 36–83, https://doi.org/10.1016/j.jphotochemrev.2017.02.001.

[4] K.C. Christoforidis, P. Fornasiero, Photocatalytic Hydrogen Production: A Rift into the Future Energy Supply, ChemCatChem 9 (2017) 1523–1544, https://doi.org/10.1002/cctc.201601659.

[5] M. Jung, J.N. Hart, D. Boensch, J. Scott, Y.H. Ng, R. Amal, Hydrogen evolution via glycerol photoreforming over Cu-Pt nanoalloys on TiO_2, Appl. Catal. A 518 (2016) 221–230, https://doi.org/10.1016/j.apcata.2015.10.040.

[6] M. Ge, J. Cai, J. Iocozzia, C. Cao, J. Huang, X. Zhang, et al., A review of TiO_2 nanostructured catalysts for sustainable H_2 generation, Int. J. Hydrogen Energy 42 (2017) 8418–8449, https://doi.org/10.1016/j.ijhydene.2016.12.052.

[7] N.S. Ibrahim, W.L. Leaw, D. Mohamad, S.H. Alias, H. Nur, A critical review of metal-doped TiO_2 and its structure–physical properties–photocatalytic activity relationship in hydrogen production, Int. J. Hydrogen Energy 45 (2020) 28553–28565, https://doi.org/10.1016/J.IJHYDENE.2020.07.233.

[8] L. Li, L. Xu, W. Shi, J. Guan, Facile preparation and size-dependent photocatalytic activity of Cu_2O nanocrystals modified titania for hydrogen evolution, Int. J. Hydrogen Energy 38 (2013) 816–822, https://doi.org/10.1016/j.ijhydene.2012.10.064.

[9] M.R. Pai, A.M. Banerjee, S.A. Rawool, A. Singhal, C. Nayak, S.H. Ehrman, et al., Solar Energy Materials & Solar Cells A comprehensive study on sunlight driven photocatalytic hydrogen generation using low cost nanocrystalline Cu-Ti oxides, Sol. Energy Mater. Sol. Cells 154 (2016) 104–120, https://doi.org/10.1016/j.solmat.2016.04.036.

[10] J. Low, J. Yu, M. Jaroniec, S. Wageh, A.A. Al-Ghamdi, Heterojunction Photocatalysts, Adv. Mater. 29 (2017) 1601694, https://doi.org/10.1002/adma.201601694.

[11] M. Muscetta, J.S. Al, G. Palmisano, R. Andreozzi, R. Marotta, S. Cimino, et al., Visible light –driven photocatalytic hydrogen production using Cu_2O/TiO_2 composites prepared by facile mechanochemical synthesis, J. Environ. Chem. Eng. 10 (2022), 107735, https://doi.org/10.1016/J.JECE.2022.107735.

[12] C.M. Pecoraro, M. Bellardita, V. Loddo, F. Di Franco, L. Palmisano, M. Santamaria, A facile way to synthesize noble metal free TiO_2 based catalysts for glycerol photoreforming, J. Ind. Eng. Chem. 118 (2023) 247–258, https://doi.org/10.1016/J.JIEC.2022.11.010.

[13] T. Wei, Y.N. Zhu, X. An, L.M. Liu, X. Cao, H. Liu, et al., Defect Modulation of Z-Scheme TiO_2/Cu_2O Photocatalysts for Durable Water Splitting, ACS Catal. 9 (2019) 8346–8354, https://doi.org/10.1021/ACSCATAL.9B01786.

[14] J.L. Chen, M.M. Liu, S.Y. Xie, L.J. Yue, F.L. Gong, K.M. Chai, et al., Cu_2O-loaded TiO_2 heterojunction composites for enhanced photocatalytic H_2 production, J. Mol. Struct. 1247 (2022), 131294, https://doi.org/10.1016/J.MOLSTRUC.2021.131294.

[15] D. Jiang, C. Xing, X. Liang, L. Shao, M. Chen, Synthesis of cuprous oxide with morphological evolution from truncated octahedral to spherical structures and their size and shape-dependent photocatalytic activities, J. Colloid Interface Sci. 461 (2016) 25–31, https://doi.org/10.1016/j.jcis.2015.09.034.

[16] M.N. Ghazzal, O. Deparis, J. De Coninck, E.M. Gaigneaux, Tailored refractive index of inorganic mesoporous mixed-oxide Bragg stacks with bio-inspired hygrochromic optical properties, J. Mater. Chem. C 1 (2013) 6202–6209, https://doi.org/10.1039/c3tc31178c.

[17] H. Jensen, A. Soloviev, Z. Li, E.G. Søgaard, XPS and FTIR investigation of the surface properties of different prepared titania nano-powders, Appl. Surf. Sci. 246 (2005) 239–249, https://doi.org/10.1016/J.APSUSC.2004.11.015.

[18] Y. Wang, Y. Lü, W. Zhan, Z. Xie, Q. Kuang, L. Zheng, Synthesis of porous Cu_2O/CuO cages using Cu-based metal–organic frameworks as templates and their gas-sensing properties, J Mater Chem A Mater 3 (2015) 12796–12803, https://doi.org/10.1039/C5TA01108F.

[19] D. Gupta, S.R. Meher, N. Illyaskutty, Z.C. Alex, Facile synthesis of Cu_2O and CuO nanoparticles and study of their structural, optical and electronic properties, J. Alloy. Compd. 743 (2018) 737–745, https://doi.org/10.1016/j.jallcom.2018.01.181.

[20] P.K. Sharma, M.A.L.R.M. Cortes, J.W.J. Hamilton, Y. Han, J.A. Byrne, M. Nolan, Surface modification of TiO_2 with copper clusters for band gap narrowing, Catal. Today (2019) 321–322, https://doi.org/10.1016/j.cattod.2017.12.002, pp. 9–17.

[21] U. Pal, Use of diffuse reflectance spectroscopy for optical characterization of un-supported nanostructures, Rev Mex Física 53 (2007) 18–22.

[22] M.K. Hossain, A.A. Mortuza, S.K. Sen, M.K. Basher, M.W. Ashraf, S. Tayyaba, et al., A comparative study on the influence of pure anatase and Degussa-P25 TiO_2 nanomaterials on the structural and optical properties of dye sensitized solar cell (DSSC) photoanode, Optik (Stuttg) 171 (2018) 507–516, https://doi.org/10.1016/j.ijleo.2018.05.032.

[23] S. Sun, Z. Yang, Recent advances in tuning crystal facets of polyhedral cuprous oxide architectures, RSC Adv. 4 (2014) 3804–3822, https://doi.org/10.1039/C3RA45445B.

[24] I.V. Bagal, N.R. Chodankar, M.A. Hassan, A. Waseem, M.A. Johar, D.H. Kim, et al., Cu_2O as an emerging photocathode for solar water splitting - A status review, Int. J. Hydrogen Energy 44 (2019) 21351–21378, https://doi.org/10.1016/j.ijhydene.2019.06.184.

[25] J. Ouyang, H. Yang, A. Tang, Shape controlled synthesis and optical properties of Cu_2O micro-spheres and octahedrons, Mater. Des. 92 (2016) 261–267, https://doi.org/10.1016/j.matdes.2015.12.012.

[26] D. Nagy, C. Chao, B. Marzec, F. Nudelman, M.C. Ferrari, X. Fan, Effect of Ag Co-catalyst on TiO_2–Cu_2O nanocomposites structure and apparent visible photocatalytic activity, J. Environ. Manage. (2020) 260, https://doi.org/10.1016/j.jenvman.2020.110175.

[27] D. Praveen Kumar, N. Lakshmana Reddy, B. Srinivas, V. Durgakumari, V. Roddatis, O. Bondarchuk, et al., Stable and active Cu_xO/TiO_2 nanostructured catalyst for proficient hydrogen production under solar light irradiation, Sol. Energy Mater. Sol. Cells 146 (2016) 63–71, https://doi.org/10.1016/J.SOLMAT.2015.11.030.

[28] C. Colbeau-Justin, M. Kunst, D. Huguenin, Structural influence on charge-carrier lifetimes in TiO_2 powders studied by microwave absorption, J. Mater. Sci. 38 (2003) 2429–2437, https://doi.org/10.1023/A:1023905102094.

[29] D. Luo, R. Yan, C. Fu, Z. Zhen, H. Yue, P. Wu, et al., $Cu^{(0)}/TiO_2$ composite byproduct from photo-reduction of acidic Cu-containing wastewater and its reuse as a catalyst, J. Water Process Eng. 32 (2019), 100958, https://doi.org/10.1016/J.JWPE.2019.100958.

[30] D. Ferrah, P. Tieu, Controllable Growth of Copper on TiO_2 Nanoparticles by Photodeposition Based on Coupled Effects of Solution Viscosity and Photoreduction Rate for Catalysis-Related Applications, ACS Appl Nano Mater 3 (2020) 5855–5861, https://doi.org/10.1021/ACSANM.0C01015/SUPPL_FILE/AN0C01015_SI_001.PDF.

[31] P. Cheng, Z. Yang, H. Wang, W. Cheng, M. Chen, W. Shangguan, et al., TiO_2 e graphene nanocomposites for photocatalytic hydrogen production from splitting water, Int. J. Hydrogen Energy 37 (2011) 2224–2230, https://doi.org/10.1016/j.ijhydene.2011.11.004.

[32] D. D'Elia, C. Beauger, J.F. Hochepied, A. Rigacci, M.H. Berger, N. Keller, et al., Impact of three different TiO_2 morphologies on hydrogen evolution by methanol assisted water splitting: Nanoparticles, nanotubes and aerogels, Int. J. Hydrogen Energy 36 (2011) 14360–14373, https://doi.org/10.1016/j.ijhydene.2011.08.007.

[33] S.G. Sanches, J.H. Flores, M.I. Pais da Silva, Influence of Ti source on the Ti-HMS photocatalyst synthesis used in a water splitting reaction, Mater. Res. Bull. 109 (2019) 82–89, https://doi.org/10.1016/j.materresbull.2018.09.021.
[34] G.D. Gesesse, C. Li, E. Paineau, Y. Habibi, H. Remita, C. Colbeau-Justin, et al., Enhanced Photogenerated Charge Carriers and Photocatalytic Activity of Biotemplated Mesoporous TiO_2 Films with a Chiral Nematic Structure, Chem. Mater. 31 (2019) 4851–4863, https://doi.org/10.1021/acs.chemmater.9b01465.
[35] H.A. Hamad, W.A. Sadik, M.M. Abd El-latif, A.B. Kashyout, M.Y. Feteha, Photocatalytic parameters and kinetic study for degradation of dichlorophenol-indophenol (DCPIP) dye using highly active mesoporous TiO_2 nanoparticles, J. Environ. Sci. (China) 43 (2016) 26–39, https://doi.org/10.1016/j.jes.2015.05.033.
[36] A. Lais, M.A. Gondal, M.A. Dastageer, F.F. Al-Adel, Experimental parameters affecting the photocatalytic reduction performance of CO_2 to methanol: A review, Int. J. Energy Res. 42 (2018) 2031–2049, https://doi.org/10.1002/er.3965.
[37] A. Olivo, V. Trevisan, E. Ghedini, F. Pinna, C.L. Bianchi, A. Naldoni, et al., CO_2 photoreduction with water: Catalyst and process investigation, Biochem. Pharmacol. 12 (2015) 86–94, https://doi.org/10.1016/j.jcou.2015.06.001.
[38] L. Clarizia, D. Russo, I. Di Somma, R. Andreozzi, R. Marotta, Hydrogen generation through solar photocatalytic processes: A review of the configuration and the properties of effective metal-based semiconductor nanomaterials, Energies 10 (2017), https://doi.org/10.3390/en10101624.
[39] M. Zanatta, L. Calvillo, J. Zheng, G.A. Rizzi, C. Durante, G. Giallongo, et al., Cu_2O/TiO_2 heterostructures on a DVD as easy&cheap photoelectrochemical sensors, Thin Solid Films 603 (2016) 193–201, https://doi.org/10.1016/j.tsf.2016.02.014.
[40] F. Plascencia-Hernández, A.L. Luna, C. Colbeau-Justin, P. Santiago, M. Garcia-Rocha, G. Valverde-Aguilar, et al., Cu_2O cubic and polyhedral structures versus commercial powder: Shape effect on photocatalytic activity under visible light, J. Saudi Chem. Soc. 23 (2019) 1016–1023, https://doi.org/10.1016/j.jscs.2019.05.007.
[41] M. Muscetta, R. Andreozzi, L. Clarizia, I. Di Somma, R. Marotta, Hydrogen production through photoreforming processes over Cu_2O/TiO_2 composite materials: A mini-review, Int. J. Hydrogen Energy 45 (2020) 28531–28552, https://doi.org/10.1016/J.IJHYDENE.2020.07.225.
[42] J. Low, B. Cheng, J. Yu, Surface modification and enhanced photocatalytic CO_2 reduction performance of TiO_2: a review, Appl. Surf. Sci. 392 (2017) 658–686, https://doi.org/10.1016/j.apsusc.2016.09.093.
[43] Y.H. Zhang, M.M. Liu, J.L. Chen, K.F. Xie, S.M. Fang, Dendritic branching Z-scheme Cu_2O/TiO_2 heterostructure photocatalysts for boosting H_2 production, J. Phys. Chem. Solid 152 (2021), 109948, https://doi.org/10.1016/J.JPCS.2021.109948.
[44] K. Kaviyarasan, V. Vinoth, T. Sivasankar, A.M. Asiri, J.J. Wu, S. Anandan, Photocatalytic and photoelectrocatalytic performance of sonochemically synthesized $Cu_2O@TiO_2$ heterojunction nanocomposites, Ultrason. Sonochem. 51 (2019) 223–229, https://doi.org/10.1016/j.ultsonch.2018.10.022.
[45] D.Y.C. Leung, X. Fu, C. Wang, M. Ni, M.K.H. Leung, X. Wang, et al., Hydrogen production over titania-based photocatalysts, ChemSusChem 3 (2010) 681–694, https://doi.org/10.1002/cssc.201000014.
[46] Q. Zhang, K. Zhang, D. Xu, G. Yang, H. Huang, F. Nie, et al., CuO nanostructures: Synthesis, characterization, growth mechanisms, fundamental properties, and applications, Prog. Mater Sci. 60 (2014) 208–237, https://doi.org/10.1016/j.pmatsci.2013.09.003.
[47] S. Lv, Y. Wang, Y. Zhou, Q. Liu, C. Song, D. Wang, Oxygen vacancy stimulated direct Z-scheme of mesoporous Cu_2O/TiO_2 for enhanced photocatalytic hydrogen production from water and seawater, J. Alloy. Compd. 868 (2021), 159144, https://doi.org/10.1016/J.JALLCOM.2021.159144.
[48] J. Low, B. Cheng, J. Yu, Surface modification and enhanced photocatalytic CO_2 reduction performance of TiO_2: a review, Appl. Surf. Sci. 392 (2016) 658–686, https://doi.org/10.1016/j.apsusc.2016.09.093.
[49] E. Szaniawska, K. Bienkowski, I.A. Rutkowska, P.J. Kulesza, R. Solarska, Enhanced photoelectrochemical CO2-reduction system based on mixed Cu_2O – nonstoichiometric TiO_2 photocathode, Catal. Today 300 (2018) 145–151, https://doi.org/10.1016/j.cattod.2017.05.099.
[50] T. Iwasita, Electrocatalysis of methanol oxidation, Electrochim. Acta 47 (2002) 3663–3674, https://doi.org/10.1016/S0013-4686(02)00336-5.
[51] P. Pootawang, N. Saito, S.Y. Lee, Discharge time dependence of a solution plasma process for colloidal copper nanoparticle synthesis and particle characteristics, Nanotechnology 24 (2013), 055604, https://doi.org/10.1088/0957-4484/24/5/055604.
[52] S. Venkatakrishnan, G. Veerappan, E. Elamparuthi, A. Veerappan, Aerobic synthesis of biocompatible copper nanoparticles: promising antibacterial agent and catalyst for nitroaromatic reduction and C-N cross coupling reaction, RSC Adv. 4 (2014) 15003–15006, https://doi.org/10.1039/C4RA01126K.
[53] G. Yu, X. Hu, D. Liu, D. Sun, J. Li, H. Zhang, et al., Electrodeposition of submicron/nanoscale Cu_2O/Cu junctions in an ultrathin $CuSO_4$ solution layer, J. Electroanal. Chem. 638 (2010) 225–230, https://doi.org/10.1016/j.jelechem.2009.11.004.
[54] Z. Xi, C. Li, L. Zhang, M. Xing, J. Zhang, Synergistic effect of Cu_2O/TiO_2 heterostructure nanoparticle and its high H_2 evolution activity, Int. J. Hydrogen Energy 39 (2014) 6345–6353, https://doi.org/10.1016/j.ijhydene.2014.01.209.
[55] A.L. Linsebigler, A.L. Linsebigler, J.T. Yates Jr, G. Lu, G. Lu, J.T. Yates, Photocatalysis on TiO_2 Surfaces: Principles, Mechanisms, and Selected Results, Chem. Rev. 95 (1995) 735–758, https://doi.org/10.1021/cr00035a013.
[56] L. Clarizia, G. Vitiello, D.K. Pallotti, B. Silvestri, M. Nadagouda, S. Lettieri, et al., Effect of surface properties of copper-modified commercial titanium dioxide photocatalysts on hydrogen production through photoreforming of alcohols, Int. J. Hydrogen Energy 42 (2017) 28349–28362, https://doi.org/10.1016/J.IJHYDENE.2017.09.093.
[57] K. Ćwieka, Z. Bojarska, K. Czelej, D. Łomot, P. Dziegielewski, A. Maximenko, et al., Zero carbon footprint hydrogen generation by photoreforming of methanol over Cu/TiO_2 nanocatalyst, Chem. Eng. J. 474 (2023), 145687, https://doi.org/10.1016/J.CEJ.2023.145687.
[58] H. Bahruji, M. Bowker, P.R. Davies, J. Kennedy, D.J. Morgan, The importance of metal reducibility for the photo-reforming of methanol on transition metal-TiO_2 photocatalysts and the use of non-precious metals, Int. J. Hydrogen Energy 40 (2015) 1465–1471, https://doi.org/10.1016/J.IJHYDENE.2014.11.097.